A CFD approach to the description of turbulent precipitation in a semi-batch Taylor-Couette reactor

14th International Congress of Chemical and Process Engineering

CHISA 2000

27 - 31 August 2000 • Praha • Czech Republic

CD-ROM
of full texts

Organised by:

Czech Society
of Chemical Engineering

CD created by:

MagicWARE

A CFD APPROACH TO THE DESCRIPTION OF TURBULENT PRECIPITATION IN A SEMI-BATCH TAYLOR-COUETTE REACTOR

Marchisio D.L., Fox R.O., Barresi A.A. and Baldi G.

paper G8.1
[# 0966]

A CFD approach to the description of turbulent precipitation in a semi-batch Taylor-Couette reactor

D.L. Marchisio[†] [1], **R.O. Fox**[‡], **A.A. Barresi**[†], **G. Baldi**[†]
[†]Dip. Scienza dei Materiali ed Ingegneria Chimica
Politecnico di Torino
C.so Duca degli Abruzzi 24, 10129, Torino, Italy
[‡]Dept. of Chemical Engineering
Iowa State University
2114 Sweeney Hall, Ames, IA 50011, USA

Abstract

Several authors have studied the predominant role of mixing and turbulent transport in reactive precipitation processes; however, different and sometimes contradictory results have been reported. In recent years, computational fluid dynamics (CFD) simulation of turbulent reactive flows has emerged as an useful tool for reactor performance prediction, design and scale-up. For example, it has been successfully applied to model mixing-controlled precipitation reactions and to predict the resulting crystal size distribution (CSD) of the dispersed phase. In this work, barium sulphate precipitation from non-premixed aqueous solutions of sodium sulphate and barium chloride has been used to validate a finite-mode probability density function (PDF) model applied to a semi-batch Taylor-Couette reactor. The Taylor-Couette reactor is made of two coaxial cylinders, with the inner one rotating and fluid contained in the annular gap. In previous works, the hydrodinamics of this reactor has been shown to be particularly interesting for control of precipitation processes. However the complexity of the flow in the annulus, and the insufficient reliability of many turbulence models for prediction of swirling flow, are well-known problems that must be addressed. In this study, in order to choose the best turbulence model for this geometry and operating conditions, a conductimetric technique has been used to measure inert tracer dispersion in the reactor, and the experimental results have been compared with the CFD predictions. After validating the flow model, a finite-mode PDF model coupled with a moment method to describe the population balance for the crystal size distribution was implemented in a commercial CFD code (FLUENT) using user-defined scalars. All the reactive precipitation simulations were carried out using the experimentally measured crystal shape factors, and kinetic data for nucleation and growth taken from literature. The reactor was first filled with sodium sulphate. Barium chloride was then added with a constant injection velocity. The crystal size distribution in samples taken from the bottom of the reactor were measured with a Coulter LS230 laser granulometer, while the residual supersaturation was measured with a conductimetric technique. These data were then used to validate the CFD model under various operating conditions, and to study the importance of the different transport processes on the crystal size distribution.

[1]Corresponding author: e-mail: marchis@athena.polito.it; fax: +390115644699

1 Introduction

Production of several materials such as catalysts, proteins, pharmaceutical products, pigments and silver halide crystals for the photographic industry involves precipitation of sparingly soluble salts. The final product quality of the materials obtained by this unit operation is strongly influenced by crystal morphology and crystal size distribution (CSD). The process involves three different steps: chemical reaction, nucleation and growth, and since the first two steps are very fast, the process is defined "mixing sensitive", in the sense that the rate is not controlled by precipitation kinetic only, but also by mixing.

The role of mixing in precipitation has been studied by several authors using different reactors in continuous and semi-batch conditions. Kim and Tarbell (1996), studying the effect of the operating conditions on the final CSD in a MSMPR, found controversial results for the effect of the stirrer speed. Pohorecky and Baldyga (1985, 1988) and Baldyga *et al.* (1990) investigated the effect of initial concentration of the reactants, feed time and stirrer speed on the solid characteristics in a semi-batch reactor. Fitchett and Tarbell (1990) working with a double feed MSMPR studied the effect of several parameters on the reactor performance.

Because of the complexity of the phenomena involved it is impossible to predict *a priori* the effect of the operating conditions, and for this reason a modeling approach provides a useful tool for interpreting experimental data. Several mechanistic models have been used, such as the Engulfment and the EDD model or the Environments model (Pohorecky and Baldyga, 1985; Garside and Tavare, 1985; Baldyga *et al.*, 1995). Wei and Garside (1997) used a CFD code to model a precipitation reactor but did not include a micromixing model, completely neglecting the role of mixing at the molecular level. On the other hand, Pipino *et al.* (1994) using a full probability density function (PDF) method and a CFD code for the flow field prediction, studied instantaneous nucleation but did not follow crystal growth. Piton *et al.* (2000), using a finite-mode PDF model coupled with a commercial CFD code studied the effect of mixing in a tubular reactor, and compared this results with the predictions obtained by Baldyga and Orciuch (1997, 1999) in a tubular reactor using a presumed-beta PDF coupled with CFD. Precipitation and agglomeration in the same system have been modelled by Marchisio *et al.* (2000b).

In this study barium sulphate precipitation in a semi-batch Taylor-Couette reactor has been described with a finite-mode PDF approach coupled with a CFD code (FLUENT). The Taylor-Couette reactor has been shown to be particularly interesting for the control of the turbulence, for its ability to provide different fluid dynamic regimes, and to create turbulence without a blade type mixer, which may cause breakage of the crystals (Barresi *et al.*, 1999). The model predictions have been validated with experimental data from the Taylor-Couette reactor. The CSD has been measured with a Coulter LS 230 laser granulometer, and the solid concentration has been calculated by measuring the residual reactants concentration using a conductimetric technique.

2 Experimental set up

In the Taylor-Couette reactor, the fluid is contained in the gap between two cylinders, and in general the inner one is rotating whereas the outer is stationary. Depending on the rotational speed of the inner cylinder several fluid dynamic regimes are achieved and a measure of the state of the flow is given by the dimensionless Taylor and Reynolds numbers, which are defined by the following

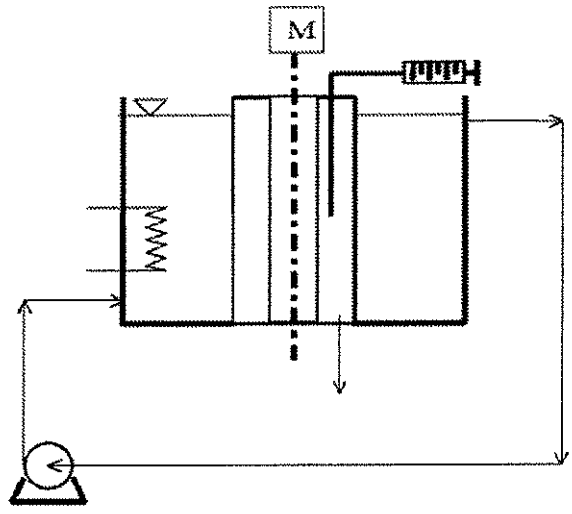

Figure 1: Experimental set up.

equations:

$$Ta = \frac{\Omega_1^2 r_1 d^3}{\nu^2} \tag{1}$$

$$Re = \frac{\Omega_1 r_1 d}{\nu} \tag{2}$$

where Ω_1 is the speed of the inner cylinder, r_1 is the radius of the inner cylinder, d is the annular gap between the two cylinders, and ν is the kinematic viscosity. When the Taylor number is lower than a critical value a laminar flow, known as the Couette flow, is achieved. An increase in the Taylor number causes a transition to a flow with toroidal vortices, known as the Taylor vortex flow (Taylor, 1923). A further increase in the Taylor number causes a transition in the following sequence: singly periodic wavy vortex flow, doubly periodic wavy vortex flow, weakly turbulent wavy vortex flow, since the fully turbulent flow without vortices is reached. Smith and Townsend (1982) estimated this transition at a Taylor number 10^5 times higher than the Taylor number of the first transition. The Taylor-Couette reactor used in this work has an inner radius (r_1) equal to 0.041 m whereas the annular gap (d) is 0.014 m, the reactor is 0.205 m high and the critical Taylor number is 1984. A sketch of the experimental setup is shown in Fig. 1.

Experiments were carried out at 25 ^{o} C. The rotational speed of the inner cylinder has been varied between 100 and 1000 rpm, corresponding to a Taylor number between 1.2×10^7 and 1.2×10^9. These values give a Taylor number ratio very close to 10^5, and thus the reactor operates in the region between turbulent vortex flow and fully turbulent flow.

Experiments for barium sulfate precipitation from aqueous solutions of sodium sulphate and barium chloride were carried out in the Taylor-Couette reactor working in semi-batch conditions. Micro-filtered water and analytical chemicals were used to prepare the solutions. The reactor was first filled with sodium sulphate solution, and barium chloride was then added with constant injection velocity. After 200 seconds, samples taken from the bottom of the reactor were analyzed. The CSD was determined using a laser granulometer (Coulter LS230) whereas the solid concentration was calculated by measuring the residual reactant concentrations with a conductimetric technique.

Table 1: Parameters investigated

N, rpm	100 - 1000
S_o	10^4 - 10^6
v, ml/min	30 - 100
f	0.1 - 0.01

The parameters investigated are:
- rotational speed of the inner cylinder (N)
- initial nominal supersaturation ($S_o = \langle c_A^0 \rangle \langle c_B^0 \rangle / k_s$), which represents the ratio of the product of the reactant concentrations in the case of complete mixing without reaction (i.e., $\langle c_A^0 \rangle$ and $\langle c_B^0 \rangle$) and the solubility product of barium sulphate (k_s)
- injection velocity (v)
- final volume ratio (f), which represents the total volume of barium chloride injected divided by the volume of sodium sulphate in the reactor

The numerical value of these parameters are reported in Table 1. In all the runs the inlet concentrations of the two reactants (c_{Ao}, c_{Bo}) and the injection time were varied to keep a stoichiometric ratio of 1:1.

3 Flow field investigation

The flow field in the reactor was investigated with a set of non-reactive tracer dispersion experiments. The reactor was first filled with micro-filtered water, and a solution of potassium chloride were then injected in the main flow direction. The injection was made using a small tube (outer diameter 2 mm, inner diameter 1 mm) located 70 mm from the top of the reactor in the middle of the annular gap, whereas the outlet of the reactor was located in the top. The outlet concentration was monitored sampling the outlet flow using a conductimetric technique. The effect of the rotational speed of the inner cylinder and of the injection velocity on macromixing was investigated, and the results confirm what has been found in previous work (Marchisio *et al.*, 1998) in a continuous Taylor-Couette reactor:
- mixing in the azimutal direction is very fast
- increasing the rotational speed of the inner cyliner the tracer concentration in the reactor is more uniform
- reducing the injection velocity the tracer concentration in the reactor is more uniform

Plotting the outlet dimensionless tracer concentration (moles leaving the reactor normalized by the total number of moles introduced) against the dimensionless injected volume a decrease in the slope of the profiles is obtained with increasing the rotational speed of the inner cylinder or with reducing the injection velocity (see Figs. 2 and 3).

The turbulent Taylor-Couette cell has been modeled using an unstructured grid with a finer resolution near the injection point, on an axial section of the reactor (2D geometry). This approach is justified by the fact that mixing in the azimuthal direction is very fast and thus the assumption of axial symmetry can be used (i.e., the mean velocity $\langle \mathbf{u} \rangle$ depends only on r and z). The modelling of complex flows, such as the Taylor-Couette flow, requires particular attention, expecially in the

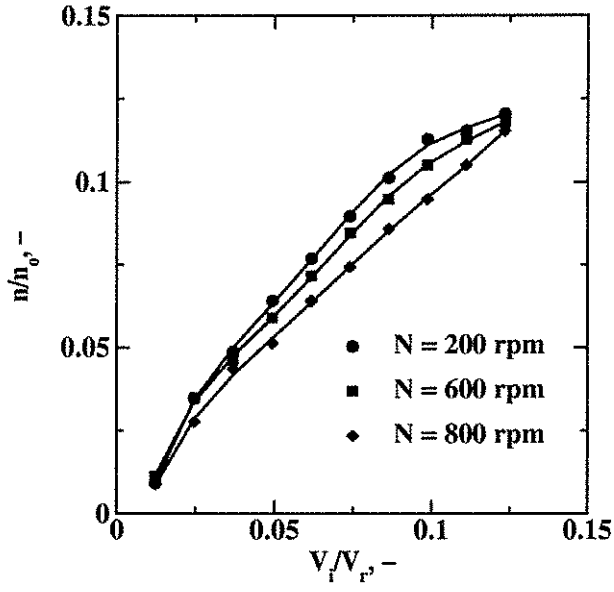

Figure 2: Dimensionless outlet tracer concentration against dimensionless injected volume for different rotational speed of inner cylinder and $v = 60$ ml/min.

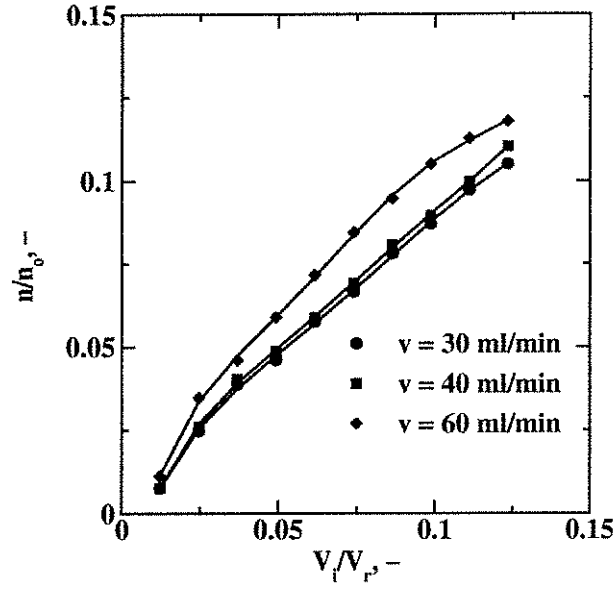

Figure 3: Dimensionless outlet tracer concentration against dimensionless injected volume for different injection velocity and $N = 600$ rpm.

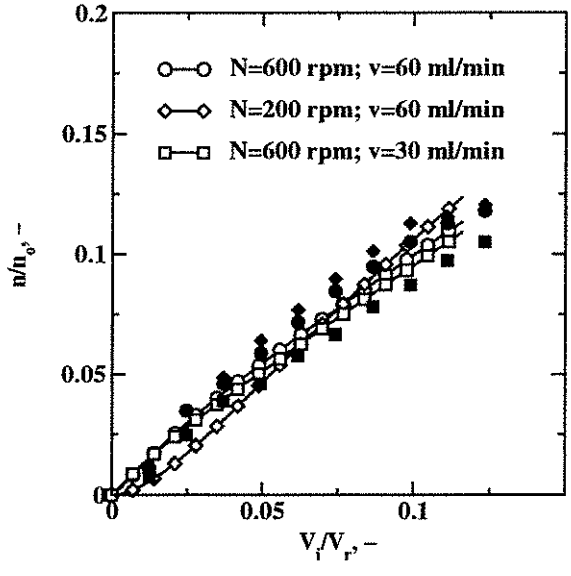

Figure 4: Comparison of CFD predictions with the RSM (open symbols) and experimental data (filled symbols) under different operating conditions.

choice of the turbulence model. For such a flow FLUENT user's guide suggests the use of two models:
- RNG $k-\epsilon$ model
- Reynolds Stress Model (RSM)

In the first model, two equations are added to the continuity and the Reynolds-averaged Navier-Stokes equations. These equations are derived using a statistical technique (renormalization group theory), and the method represents a refinement of the standard $k-\epsilon$ method, with enhanced accuracy, in particular for swirling flow. The second one is the Reynolds Stress Model (RSM), which is the most elaborate turbulence model available in FLUENT. In this model the isotropic eddy-viscosity hypothesis is abandoned, and four (2D) or seven (3D) equations are added to the Navier-Stokes/continuity equations. The added equations are the Reynolds stress transport equations and the equation for the dissipation rate [for details on the two models, see Valerio *et al.* (1998)]. The ability of prediction of a CFD code, should be validated by rigorous comparison of the predicted flow variables (i.e., Reynolds-averaged velocities, turbulent kinetic rate, and turbulent dissipation rate) with the experimental data. However a simpler approach such as comparison of dispersion of an inert tracer can give usefull information on the flow field. For this reason simulation results obtained carrying out a set of time-dependent simulations, with a local injection of tracer in the inlet zone, have been compared with experimental data. Both models predict a flow with counter-rotating vortices, even in number, but with different local value of Reynolds-averaged velocities and turbulence properties. Although it is difficult to discriminate between the two turbulence models that were used, comparison of experiments and predictions indicates that unlike the RNG $k-\epsilon$ model, the RSM gives the correct qualitative prediction of the influence of the operating conditions (see Fig. 4).

4 Micromixing model

A finite-mode PDF model has been chosen to model micromixing. In this approach every cell of the computational domain contains N_e different modes or environments, which corresponds to a discretization of the composition PDF in a finite set of delta functions (Fox, 1998):

$$f_\phi(\psi;\mathbf{x},t) \equiv \sum_{n=1}^{N_e} p_n(\mathbf{x},t) \prod_{\alpha=1}^{m} \delta(\psi_\alpha - \phi_\alpha^{(n)}(\mathbf{x},t)) \tag{3}$$

where $f_\phi(\psi;\mathbf{x},t)$ is the joint PDF of all scalars (e.g., concentrations, moments, etc.) appearing in the precipitation model, $p_n(\mathbf{x},t)$ is the probability of mode n, $\phi_\alpha^{(n)}(\mathbf{x},t)$ is the value of scalar α corresponding to mode n, N_e is the total number of modes, and m is the total number of scalars. By definition, the probabilities sum to unity and the average value of any scalars is defined by integration with respect to ψ. Without loss of generality we will take the first scalar to be the mixture fraction [$\phi_1(\mathbf{x},t) \equiv \xi(\mathbf{x},t)$]. This approach has been successfully used to model micromixing in precipitation, and because the first results showed that three modes are sufficient to work with good accuracy, we will take $N=3$ (Piton *et al.*, 2000).

The 3-mode PDF model can be thought of as the discretization of the reactive system in three environments, where Environments 1 and 2 contain unmixed reactants A and B, respectively, and reaction/particle formation occurs in Environment 3. The scalar transport equations for the probabilities of modes 1 and 2, and for the weighted mixture fraction in Environment 3 ($s_3 = \xi^{(3)} p_3$) are (repeated indices imply summation)

Table 2: Model constants used in the simulations

C_μ	0.09
Sc_t	0.7
C_ϕ	0.5

$$\frac{\partial p_1}{\partial t} + \frac{\partial}{\partial x_i}(\langle u_i \rangle p_1) = \frac{\partial}{\partial x_i}\left(\Gamma_t \frac{\partial p_1}{\partial x_i}\right) + \gamma_t p_3 - \gamma_s p_1(1-p_1), \tag{4}$$

$$\frac{\partial p_2}{\partial t} + \frac{\partial}{\partial x_i}(\langle u_i \rangle p_2) = \frac{\partial}{\partial x_i}\left(\Gamma_t \frac{\partial p_2}{\partial x_i}\right) + \gamma_t p_3 - \gamma_s p_2(1-p_2), \tag{5}$$

$$\frac{\partial s_3}{\partial t} + \frac{\partial}{\partial x_i}(\langle u_i \rangle s_3) = \frac{\partial}{\partial x_i}\left(\Gamma_t \frac{\partial s_3}{\partial x_i}\right) - \gamma_t p_3(\xi^{(1)} + \xi^{(2)}) + \tag{6}$$

$$\gamma_s p_1(1-p_1)\xi^{(1)} + \gamma_s p_2(1-p_2)\xi^{(2)}.$$

where $p_3 = 1-p_1-p_2$, $\langle u_i \rangle$ is the mean velocity in the i^{th} direction, Γ_t is the turbulent diffusivity modeled as

$$\Gamma_t = \frac{C_\mu}{Sc_t}\frac{k^2}{\epsilon}, \tag{7}$$

whereas γ_s and γ_t are respectively the micromixing rate, and the spurious dissipation rate. The last one is required to eliminate spurious scalar dissipation resulting from the finite-mode representation, by setting γ_t as follows:

$$\gamma_t = \frac{2\Gamma_t}{1-2\xi^{(3)}(1-\xi^{(3)})}\frac{\partial \xi^{(3)}}{\partial x_i}\frac{\partial \xi^{(3)}}{\partial x_i}. \tag{8}$$

The term γ_s is the scalar dissipation rate due to micromixing. Writing a relationship between turbulent dissipation rate and turbulent frequency (ε/k) as proposed by Fox (1995, 1997, 1999) the following equation is obtained:

$$\gamma_s = C_\phi \varepsilon/k \tag{9}$$

where C_ϕ is a constant that for fully-developed turbulence is of the order of unity. In this work, in order to account for the fact that the scalar field near the injection point is not fully developed we use a value of $C_\phi = 0.5$. However, it is found that the simulation results are relatively insensitive to the choice of the value of C_ϕ. The numerical values of the constants used in the simulations are reported in Table 2. The model equations are added to FLUENT as user-defined scalars. For every user-defined scalar a transport equation of the form

$$\rho\frac{\partial\phi_k}{\partial t}+\frac{\partial}{\partial x_i}\left(\rho\langle u_i\rangle\phi_k-\rho\Gamma_k\frac{\partial\phi_k}{\partial x_i}\right)=S_{\phi_k} \tag{10}$$

is solved, where ϕ_k is the k^{th} scalars, ρ is the fluid density and Γ_k, and S_{ϕ_k} are the diffusivity and the source term for the k^{th} scalar, respectively. In this work the diffusivity Γ_k has been set equal to the turbulent diffusivity (Γ_t) for all scalars. Note that the source term must be consistent with the dimensions of the other terms in Eq. 10. For this reason the source terms appearing in Eqs. 4-6 are multiplied by the fluid density. For example, the source term for the first scalar (p_1) is given by

$$S_{p_1}=\rho\left[\gamma_t p_3-\gamma_s p_1(1-p_1)\right]. \tag{11}$$

Turbulent reactive flows can be more simply described in terms of the reaction progress variable and the mixture fraction variable. The mixture fraction is used to describe mixing between two feed streams in a reactor (Fox, 1996). For a simple reaction (i.e., $A+B\rightarrow C$) in the case of two non-premixed feeds, the mixture fraction is a conserved scalar defined as follows:

$$\xi=\frac{c_A-c_B+c_{Bo}}{c_{Ao}+c_{Bo}} \tag{12}$$

where c_{Ao} and c_{Bo} are the inlet concentrations of the two reactants in their separate feed streams. From Eq. 12 it is clear that the mixture fraction is equal to 1 in one feed stream ($c_A=c_{Ao}; c_B=0$) and 0 in the other ($c_A=0; c_B=c_{Bo}$). Using this approach the relationships between concentrations, mixture fraction, and reaction progress variable (Y) for finite rate chemical reaction are

$$\frac{c_A}{c_{Ao}}=\xi-\xi_s Y, \qquad \frac{c_B}{c_{Bo}}=(1-\xi)-(1-\xi_s)Y. \tag{13}$$

These relationships are included in the two limit cases of non-reacting system and istantaneous reaction. In the case of a non-reacting system, the relationships between the mixture fraction and the reactant concentrations are:

$$\frac{c_A^0}{c_{Ao}}=\xi, \quad \frac{c_B^0}{c_{Bo}}=1-\xi \tag{14}$$

where c_A^0 and c_B^0 are the reactant concentrations in the case of mixing without reaction. In the case of instantaneous reaction, the two reactants cannot coexist at the same point, and thus the mixture fraction is related to the reactant concentrations as follows:

$$\frac{c_A^\infty}{c_{Ao}}=\begin{cases}0 & \text{for } \xi<\xi_s\\ \frac{\xi-\xi_s}{1-\xi_s} & \text{for } \xi\geq\xi_s\end{cases}, \qquad \frac{c_B^\infty}{c_{Bo}}=\begin{cases}1-\frac{\xi}{\xi_s} & \text{for } \xi<\xi_s\\ 0 & \text{for } \xi\geq\xi_s\end{cases} \tag{15}$$

where

$$\xi_s=\frac{c_{Bo}}{c_{Ao}+c_{Bo}}. \tag{16}$$

Note that Y is null for all inlet/initial conditions, because it is proportional to the amount of reaction product. Thus, in order to close the problem, a transport equation for the mean reaction progress variable $\langle Y\rangle$ must be added:

$$\frac{\partial\langle Y\rangle}{\partial t}+\frac{\partial}{\partial x_i}(\langle u_i\rangle\langle Y\rangle)=\frac{\partial}{\partial x_i}\left(\Gamma_t\frac{\partial\langle Y\rangle}{\partial x_i}\right)+\frac{p_3 S(c_A^{(3)},c_B^{(3)})}{\xi_s c_{Ao}} \tag{17}$$

where $S(c_A^{(3)}, c_B^{(3)})$ is the source term for the chemical reaction, and $c_A^{(3)}$ and $c_B^{(3)}$ are defined in terms of s_3, p_3 and $\langle Y \rangle$ by

$$\frac{c_A^{(3)}}{c_{Ao}} = \frac{s_3 - \xi_s \langle Y \rangle}{p_3}, \qquad \frac{c_B^{(3)}}{c_{Bo}} = \frac{p_3 - s_3 - (1 - \xi_s)\langle Y \rangle}{p_3}. \tag{18}$$

Micromixing will influence the predictions of the model in regions where $p_3 < 1$, whereas in perfect micromixing regions $p_3 = 1$. The local reactant concentration will thus be greater then the mean concentration whenever $p_3 < 1$, resulting in increased rates of nucleation and growth.

The reactive system can thus be studied using Eq. 4 and 5 to describe the spatial and temporal evolution of the volume fractions of Environments 1 and 2, Eq. 6 to describe the evolution of the mixture fraction in Environment 3, and Eq. 17 to account for the chemical reaction in Environment 3. Equation 18 is used to relate the reactant concentrations to the mixture fraction and the mean reaction progress variable. The problem will thus be closed once a functional form has been specified for $S(c_A, c_B)$.

5 Population balance and precipitation kinetic

The population balance is a continuity statement expressed in terms of the particle number density $n(L; \mathbf{x}, t)$ that is a function of time (t), position ($\mathbf{x}$) and particle dimension (L) (Randolph and Larson, 1988). This function multiplied by an infinitesimal increment in the particle dimension [i.e., $n(L; \mathbf{x}, t)dL$] represents the number density of particles with dimensions between L and $L + dL$. In order to obtain a simpler expression, the population balance can be expressed in terms of the moments of the particle number density function. With this approach the governing equations are (Rivera and Randolph, 1978)

$$\frac{\partial m_0}{\partial t} + \frac{\partial}{\partial x_i}(\langle u_i \rangle m_0) = \frac{\partial}{\partial x_i}\left(\Gamma_t \frac{\partial m_0}{\partial x_i}\right) + B(c_A^{(3)}, c_B^{(3)})p_3, \tag{19}$$

$$\frac{\partial m_1}{\partial t} + \frac{\partial}{\partial x_i}(\langle u_i \rangle m_1) = \frac{\partial}{\partial x_i}\left(\Gamma_t \frac{\partial m_1}{\partial x_i}\right) + G(c_A^{(3)}, c_B^{(3)})m_0, \tag{20}$$

$$\frac{\partial m_2}{\partial t} + \frac{\partial}{\partial x_i}(\langle u_i \rangle m_2) = \frac{\partial}{\partial x_i}\left(\Gamma_t \frac{\partial m_2}{\partial x_i}\right) + 2G(c_A^{(3)}, c_B^{(3)})m_1, \tag{21}$$

$$\frac{\partial m_3}{\partial t} + \frac{\partial}{\partial x_i}(\langle u_i \rangle m_3) = \frac{\partial}{\partial x_i}\left(\Gamma_t \frac{\partial m_3}{\partial x_i}\right) + 3G(c_A^{(3)}, c_B^{(3)})m_2, \tag{22}$$

$$\frac{\partial m_4}{\partial t} + \frac{\partial}{\partial x_i}(\langle u_i \rangle m_4) = \frac{\partial}{\partial x_i}\left(\Gamma_t \frac{\partial m_3}{\partial x_i}\right) + 4G(c_A^{(3)}, c_B^{(3)})m_3. \tag{23}$$

where B is the nucleation rate, G is the growth rate, m_j is the mean value of the jth moment of the particle number density function (i.e., $m_j = p_3 m_j^{(3)}$).

The first five moments are computed in Environment 3 where the reaction occurs, and can be used to express the solid concentration and the mean crystal size as follows

$$c_C = \frac{\rho_s k_v m_3}{M}, \tag{24}$$

$$d_{43} = \frac{m_4}{m_3}, \tag{25}$$

where ρ_s is the crystal density, k_v is the volume shape factor, and M is the molecular weight of the crystal. The chemical source term appearing in Eq. 17 can be expressed in terms of m_2 and G as follows:

$$p_3 S(c_A, c_B) = \frac{3\rho_s k_v m_2}{M} G(c_A, c_B). \tag{26}$$

In order to close the problem an expression for the growth and the birth rate, and a numerical value for the shape factor must be supplied. Barium sulfate precipitation from aqueous solution has been widely used to validate micromixing models and to study the influence of mixing. In the literature several kinetic expressions have been proposed. Baldyga and coworkers (Baldyga *et al.*, 1995) used a power law for the nucleation rate:

$$B(c_A, c_B) = \begin{cases} 2.83 \times 10^{10} \Delta c^{1.775} \quad (1/\mathrm{m^3 s}) \quad \text{for} \quad \Delta c < 10 \text{ mol/m}^3 \textit{ (heterogeneous)} \\ 2.53 \times 10^{-3} \Delta c^{15} \quad (1/\mathrm{m^3 s}) \quad \text{for} \quad \Delta c > 10 \text{ mol/m}^3 \textit{ (homogeneous)} \end{cases} \tag{27}$$

where $\Delta c = \sqrt{c_A c_B} - \sqrt{k_s}$, and k_s is the solubility product of barium sulphate (at room temperature k_s=1.14 $\times$ 10^{-4} mol^2/m^6). Starting from the results obtained by Nielsen (1969), Aoun *et al.* (1996) found an expression for the growth rate which takes into account the effect of non-stoichiometric conditions:

$$G(c_A, c_B) = k_G (c_A - \sqrt{k_s})^{1.15} (c_B - \sqrt{k_s})^{0.95} \quad (\mathrm{m/s}) \tag{28}$$

where

$$k_G = \begin{cases} 1.05 \times 10^{-5} 10^{-1.57/R_o} & \text{for } R_o > 1 \\ 2.73 \times 10^{-5} R_o^{-1.99 R_o} & \text{for } R_o \leq 1 \end{cases} \tag{29}$$

and $R_o = c_A/c_B$.

Pagliolico *et al.* (1999) analized some SEM photographs of barium sulphate crystals obtained in a continuous Taylor-Couette reactor. They found that the mean crystal size given by the particle sizer (Malvern LS230) is intermediate between the values of the length and the width of the crystals, but generally closer to the last one. Using this characteristic dimension they obtained several values of shape factors for several morphologies. Marchisio *et al.* (2000a), solving the population balance for a simplified system, studied the influence of this factor on the mean crystal size, and proposed an average value for the volume shape factor (k_v=0.06) for crystals obtained in the Taylor-Couette reactor.

6 Results and Discussion

The reactor was modelled in an axial section in semi-batch condition, using three different grids. The three grids were generated with different resolution near the injection point in order to find the grid-indipendent solution. The turbulent flow field was solved first, until a steady-state solution was achieved. Using this flow field, a total of nine transport equations (Eqs. 4-6, 17, 19-23) were solved as user-defined scalars in FLUENT. The initial conditions for the computational domain inside the reactor are as follows:

$$p_1 = 0, \quad p_2 = 1, \quad s_3 = \langle Y \rangle = m_0 = m_1 = m_2 = m_3 = m_4 = 0, \tag{30}$$

whereas at the inlet point:

$$p_1 = 1, \quad p_2 = 0, \quad s_3 = \langle Y \rangle = m_0 = m_1 = m_2 = m_3 = m_4 = 0. \tag{31}$$

Barium chloride is the reactant in Environment 1 whereas sodium sulphate is the reactant in Environment 2. At the beginning of the simulation, the reactor is occupied by Environment 2 except at the injection point. During injection Environment 1 enters into the reactor and due to mixing Environment 2 starts to disappear. After approximately one second, Environment 3 has completely taken the place of Environment 2, except near the injection zone, where Environment 3 will not be equal to one until the injection is finished.

In Figs. 5 and 6, the volume-averaged values of the volume fractions of Environments 1 and 2 against time, are reported. The injection velocity has little effect on the temporal evolution of Environment 2, but has a strong effect on the temporal evolution of Environment 1. In fact, Fig. 5 shows that different injection velocities imply different injection times, and moreover the value of the volume fraction of Environment 1 during the injection increases with decreasing injection velocity. Note, however that even at high injection velocities the volume fraction of Environment 1 remains relatively small.

From these observations, we can draw the following conclusions concerning mixing in this reactor. Within 1 second (see Fig. 5), large scale gradients due to the initial conditions are eliminated. The reactor then operates in a steady-state regime until the injection is finished (see Fig. 5). During this period, the largest gradients (and hence micromixing) are concentrated in a small volume surrounding the injection point. At the end of the injection period, all gradients in mixture are quickly eliminated and the system behaves like a perfectly mixed batch reactor. Thus, despite the fact that the micromixing parameter C_ϕ was chosen smaller than the value for fully-developed turbulence, the effect of micromixing on the overall process was found to be very small.

The time step used in the time-dependent simulations was varied depending on the operating conditions. In fact, it was found that when the concentrations of the reactants is locally high the problem becomes stiff, and thus the time step has to be sufficiently small to avoid floating point errors. For low values of the initial nominal supersaturation ratio (S_o) and high values of the volume ratio (f), the time step had been kept constant and equal to 1 second, whereas at high values of the initial nominal supersaturation ratio and low values of the volume ratio, the time step has been initially fixed to 10^{-4} seconds. As soon as the simulation had successfully completed one time iteration, the time step was increased to 0.1 second. The effect of the operating conditions on supersaturation (S), total particle number density (m_0) and mean crystal size (d_{43}) have been studied. The reported values of these variables are volume-averaged values over all the reactor. In the case of precipitation, the interpretation of the results is often difficult and controversial because of the many phenomena involved [i.e., mixing at various scales (macro-, meso- and micro-mixing),

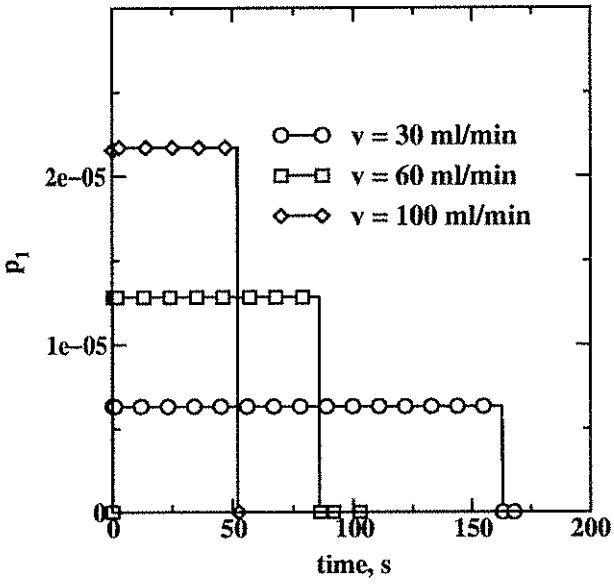

Figure 5: Volume-averaged volume fraction of Enviroments 1 for three different injection velocities ($N = 500$ rpm).

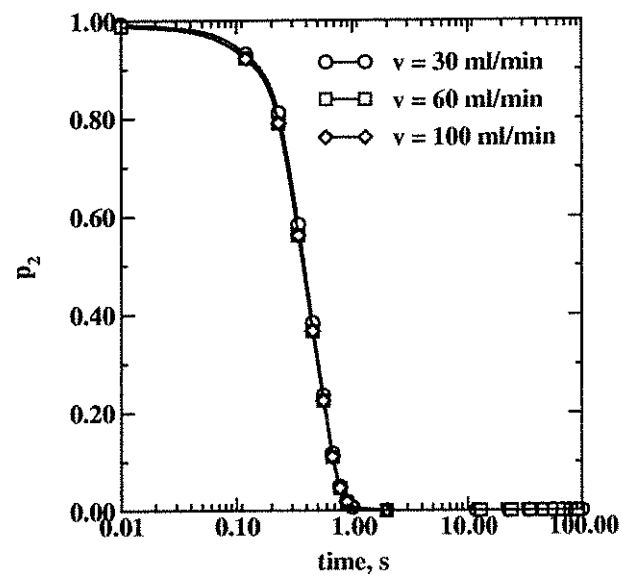

Figure 6: Volume-averaged volume fraction of Enviroments 2 for three different injection velocities ($N = 500$ rpm)

nucleation and growth]. Because of its strong non-linearity, nucleation is more favored by high supersaturation than growth, but often this effect is confined in such small area of the reactor that the total particle number density and the mean crystal size are relatively insensitive to micromixing (Piton *et al.*, 2000). Moreover, the effect of varying a single parameter can be different depending on the controlling process. For example, an increase in the intensity of mixing can reduce the volume-average intensity of segregation of the reactant favoring nucleation, or reduce the local peak of supersaturation disfavoring it.

Effect of injection velocity. In Fig. 7 the volume-averaged supersaturation profiles are reported for three injection velocities. The observed discontinuity in the derivative of the profile occurs at the end of the injection period. From the figure is clear that increasing the injection velocity results in a higher peak of supersaturation. However, the supersaturation subsequently decreases more rapidly due to crystal growth. Overall, the supersaturation is kept at a higher time-averaged value with low injection velocity and this effect causes the formation of a higher number of particles (Fig. 8) with a lower dimension (Fig. 9) under these conditions. A comparison with the experimental data for the volume-averaged mean crystal size at the end of the reaction is reported in Fig. 10, and good agreement has been found.

Effect of rotation speed. The effect of the rotational speed of the impeller on the crystal size has been analyzed by several authors, and different results and conclusions have been found. Kim and Tarbell (1996) found a maximum of the mean crystal size versus the stirrer speed, while Phillips *et al.* (1999) and Fitchett and Tarbell (1990) found a monotonic increase. Differently from what observed in the continuous apparatus (Barresi *et al.*, 1999), in the semi-batch Taylor-Couette reactor both the model and the experimental data show a decrease of the mean crystal size when plotted against the rotational speed of the internal cylinder (Fig. 11). This effect might be caused by enhanced macromixing, which reduces the degree of segregation of the reactants and as a consequence increases the peak of volume-averaged supersaturation (see Fig. 12). The final effect is to produce a slightly higher number of particles, because of the favored nucleation, but with a

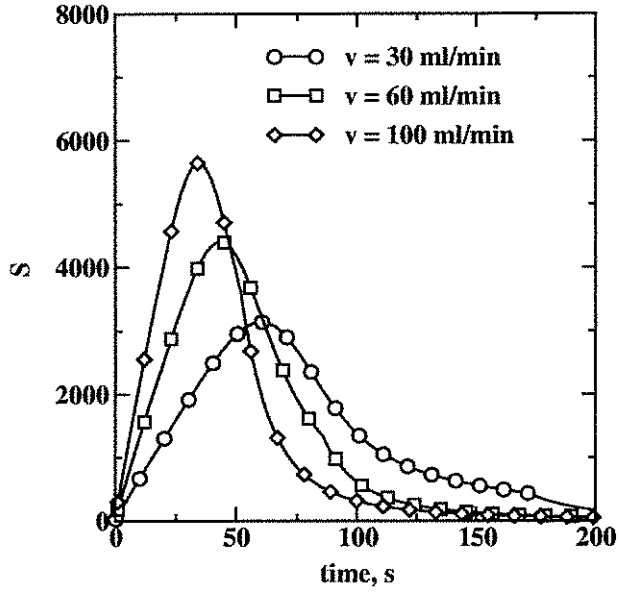

Figure 7: Volume-averaged supersaturation versus time for three injection velocities ($N = 500$ rpm, $f = 0.1$, $\log(S_o) = 4$).

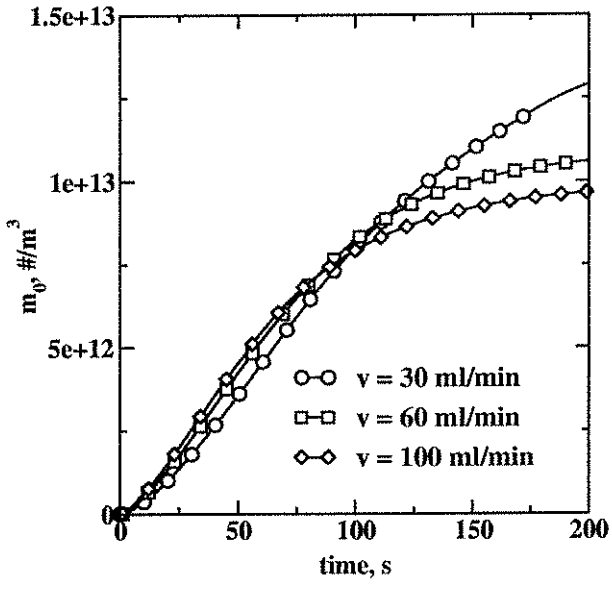

Figure 8: Volume-average total particle number density versus time for three injection velocities ($N = 500$ rpm, $f = 0.1$, $\log(S_o) = 4$).

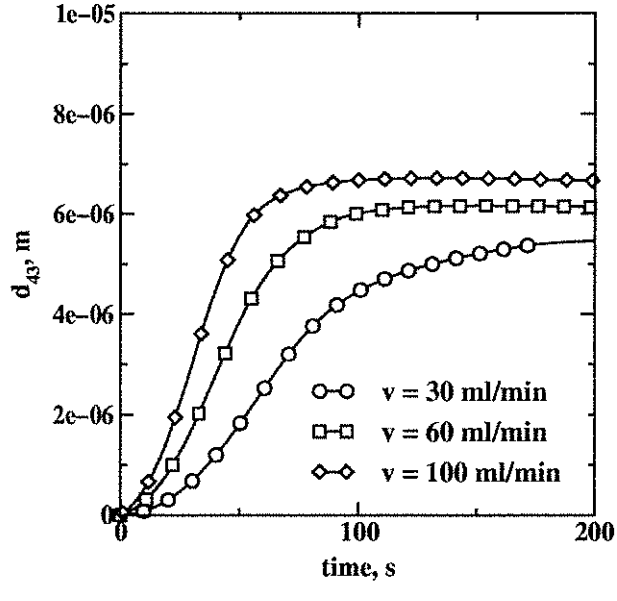

Figure 9: Volume-averaged mean crystal size versus time for three injection velocities ($N = 500$ rpm, $f = 0.1$, $\log(S_o) = 4$).

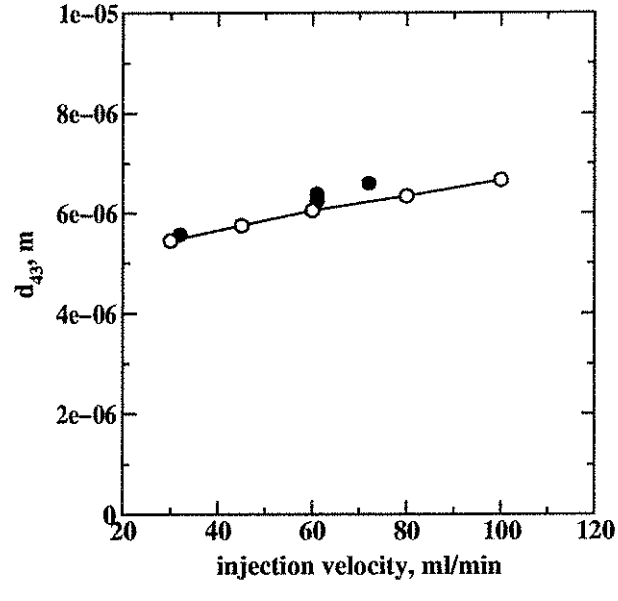

Figure 10: Final mean crystal size versus injection velocity ($N = 500$ rpm, $f = 0.1$, $\log(S_o) = 4$). Open symbols: CFD prediction. Filled symbols: experimental data.

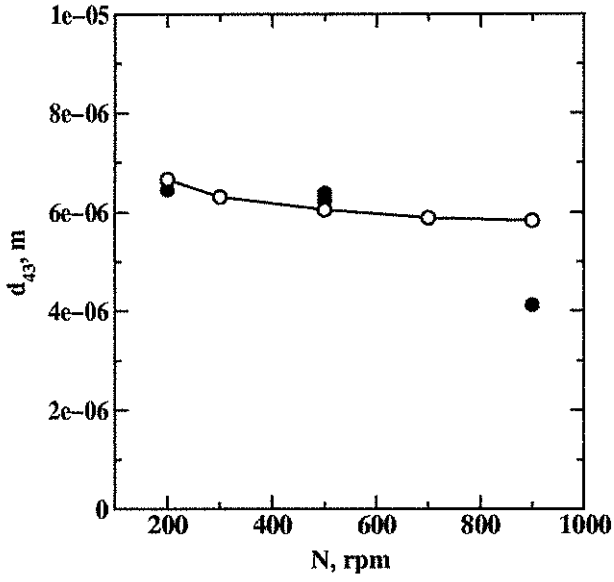

Figure 11: Final mean crystal size versus speed of the internal cylinder ($v = 60$ ml/min, $f = 0.1$, $\log(S_o)$=4). Open symbols: CFD prediction. Filled symbols: experimental data.

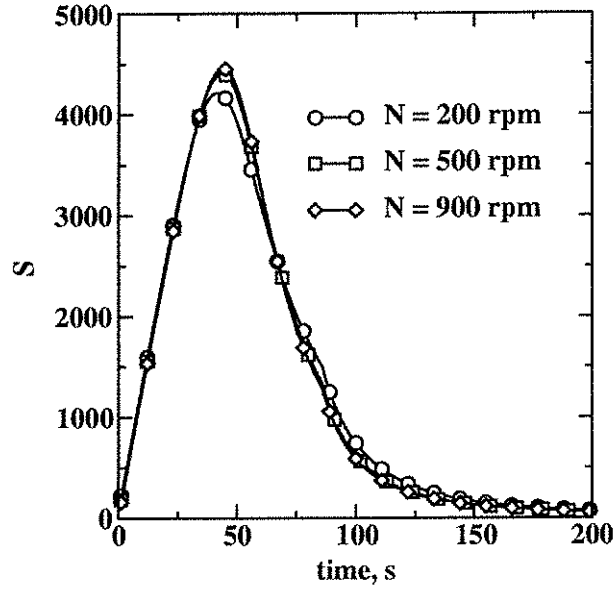

Figure 12: Volume-averaged supersaturation versus time for three speeds of the internal cyliner ($v = 60$ ml/min, $f = 0.1$, $\log(S_o)$=4).

smaller dimension (see Fig. 13). In Fig. 14 a plot of the solids concentration against the speed of the internal cylinder is reported. The figure shows that the rotational speed does not significantly affect the final yield. The same behavior has also been found for all the other parameters.

Effect of initial nominal supersaturation. The effect of the initial nominal supersaturation ratio (S_o) has been studied for values between 10^4 and 10^6. As it is possible to see from Fig. 15, increasing this ratio the peak of the supersaturation is increased, resulting in a larger number of particles, that grow rapidly due to the enhanced growth rate, and remove the reactants. It has to be highlighted that for the highest value of S_o, the reactant concentrations reach the equilibrium value ($\sqrt{k_s}$) and thus no more growth is detected (see the flat line starting from $t = 140s$ in Figs. 15).

The comparison with the experimental data is reported in Fig. 17 for different initial nominal supersaturation ratios. Since under these conditions the growth rate is favored over the nucleation rate, both model and experiments show an increase in the mean crystal size with increasing S_o. However the model over-predicts the rate of increase, because of the strong segregation in the system due to the vortices, that causes poor macromixing. This result, once again, shows the importance of an accurate knowledge of the flow field, in order to predict its effect on the final CSD.

Effect of Reactant Volume Ratio. The effect of the reactant volume ratio has been studied for two different values of the initial nominal supersaturation ratio [$\log(S_o)$=4 and 6]. The results are reported in Fig. 18 and the model predictions for $\log(S_o)$=4 are compared with experimental data. To be consistent with our earlier terminology, the volume ratio (f) is the volume average of the mean mixture fraction $\langle\xi\rangle$ at the end of the injection period, in fact it represents the final volume fraction of fluid injected into the reactor. In order to maintain a 1:1 stoichiometric ratio, decreasing f results in a higher concentration of the reactant over a shorter injection time at the same flow rate. This results in a significant increase of the local supersaturation near the injection

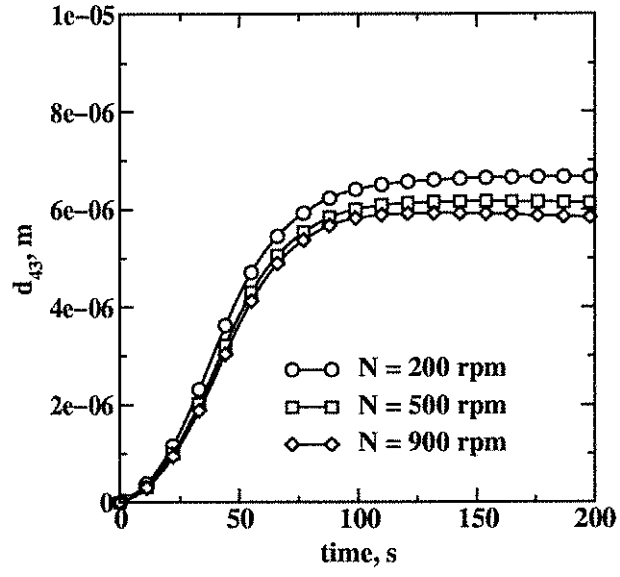

Figure 13: Volume-averaged supersaturation versus time for three speeds of the internal cyliner (v = 60 ml/min, f = 0.1, log(S_o)=4).

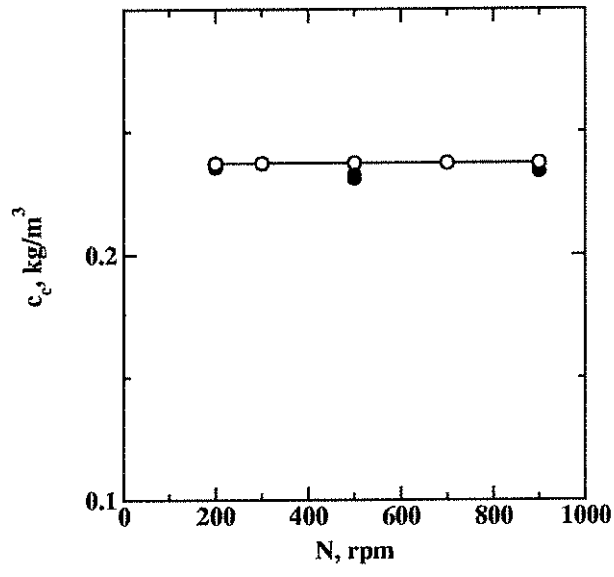

Figure 14: Final solid concentration versus speed of the internal cylinder (v = 60 ml/min, f = 0.1, log(S) = 4). Open symbols: CFD prediction. Filled symbols: experimental data.

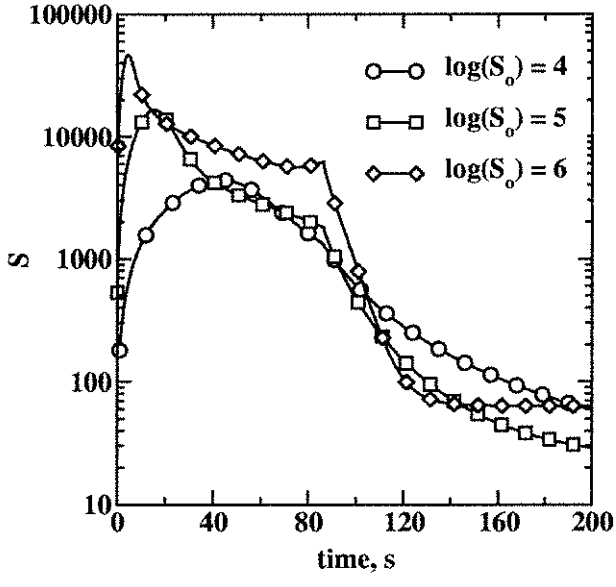

Figure 15: Volume-averaged supersaturation versus time for three initial nominal supersaturation ratios (v = 60 ml/min, f = 0.1, N = 500 rpm).

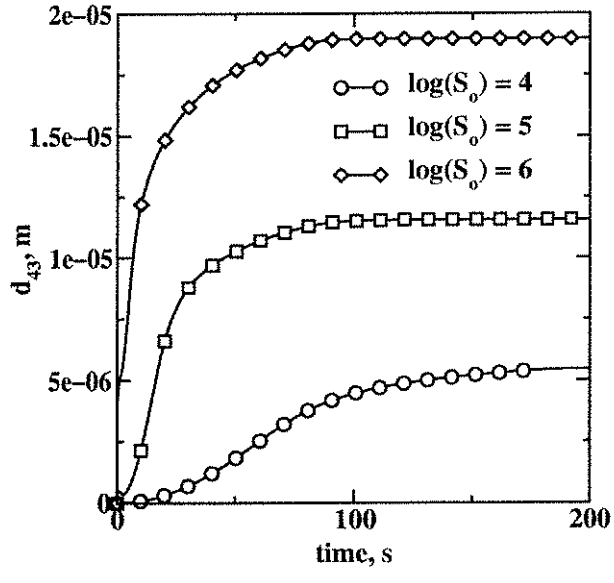

Figure 16: Volume-averaged mean crystal size versus time for three initial nominal supersaturation ratios (v = 60 ml/min, f = 0.1, N = 500 rpm).

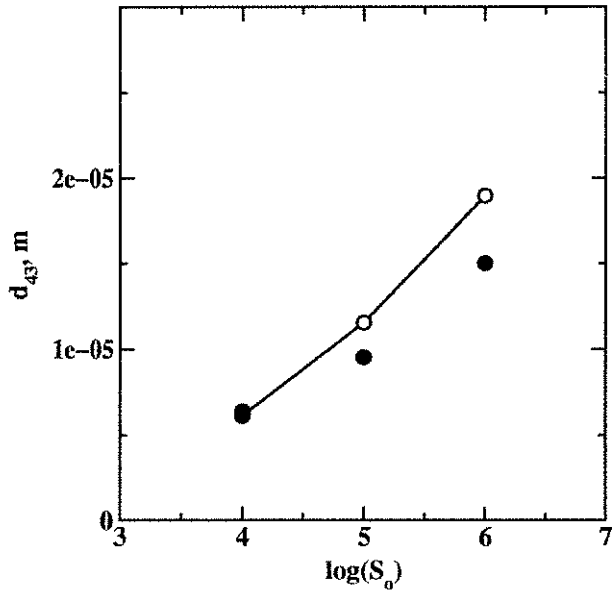

Figure 17: Comparison with experimental data for the final mean crystal size versus the initial nominal supersaturation ratio (v = 60 ml/min, f = 0.1, N = 500 rpm). Open symbols: CFD prediction. Filled symbols: experimental data.

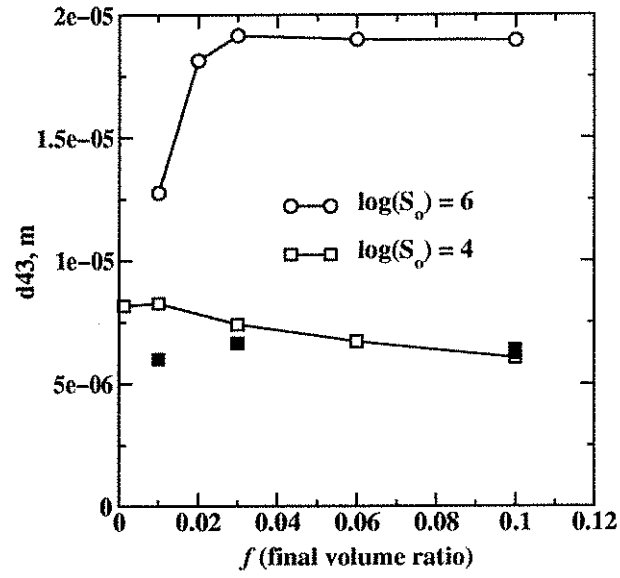

Figure 18: Final mean crystal size versus mean mixture fraction for two different initial supersaturation ratios (N = 500 rpm, v = 60 ml/min). Open symbols: CFD predictions. Filled symbols: experimental data.

point. Depending on the initial nominal supersaturation, this local increase can favor nucleation or growth. At low values of the initial nominal supersaturation ratio [log(S_o)=4], the local value of the supersaturation is not high enough to induce homogeneous nucleation, and this results in a smaller number of crystals with higher dimension. However, when the initial nominal supersaturation ratio is increased to 10^6, the local value of the supersaturation leads to homogeneous nucleation and a higher number of particles with lower dimension are produced. Furthermore, a decrease in the mean crystal size is observed in the simulations for volume ratios lower than 0.01 for log(S_o)=4, and 0.03 for log(S_o)=6. In the first case, only when the volume ratio is lower than 0.01 is the local value of the supersaturation high enough to favor nucleation over growth. In the second case, this condition is satisfied for volume ratios less than 0.1. The fact that the mean crystal size starts to decrease with a decreasing volume ratio at lower values of this parameter is due to the segregation of the fresh reactants. Only when the volume ratio is small enough to have a short injection time, will the introduction of the reactant be faster than the growth process, so that during the injection the high local supersaturation favors nucleation.

7 Conclusions

A finite-mode PDF model coupled with a CFD code (FLUENT) has been used to model precipitation of barium sulphate in a semi-batch Taylor-Couette reactor. The CSD has been calculated in terms of the first five moments of the CSD and the model has been validated with experimental data. The effects of various operating conditions (speed of the internal cylinder, injection velocity, initial nominal supersaturation, reactants volume ratio) have been investigated. The results show that the precipitation reaction is strongly influenced by the local value of supersaturation at high

reactant concentrations. Mixing at various scales has been found to be the controlling phenomenon and in particular the vortical structure of the flow in the Taylor-Couette reactor favors the role of macromixing. The use of time-dependent CFD has been shown to be a feasible modeling approach for predicting the behavior of the reactor. Although the flow field has been validated only through tracer experiments, and no direct information on the turbulent flow field are available for model validation, the overall agreement with experimental data is satisfactory. Nevertheless, deeper investigation of the flow field will be required in order to completely verify the effect of turbulence parameters on the degree of mixing at various scales in the reactor.

Acknowledgements

The research has been partially supported by an Italian National research project (MURST 40% - Multiphase reactors: hydrodynamics analysis and solid-liquid analysis).

Notation

B	nucleation rate, $1/m^3s$
c_A	barium chloride concentration, mol/m^3
c_B	sodium sulphate concentration, mol/m^3
c_C	weighted solid concentration in mode 3, kg/m^3
C_μ	turbulent constant
C_ϕ	micromixing constant
d	annular gap between the cylinders, m
d_{43}	mean crystal size, m
f	final volume ratio between the two reactant solutions
$f_\phi(\psi; \mathbf{x}, t)$	joint probability density function
G	crystal growth rate, m/s
k	turbulent kinetic energy, m^2/s^2
k_s	barium sulphate solubility product, mol^2/m^6
k_v	volume shape factor
L	particle dimension, m
m_j	weighted j^{th} moment of the crystal size distribution in mode 3
M	barium sulphate molecular weight, kg/mol
$n(L; \mathbf{x}, t)$	particle number density function
N	rotational speed of the inner cylinder, rpm
N_e	number of modes/environments
p_n	probability of mode n
r_1	radius of the inner cylinder, m
R_o	reactant concentrations ratio
Re	dimensionless rotational Reynolds number
s_3	weighted mixture fraction in mode 3
Sc_t	turbulent Schimdt number
S_o	initial nominal supersaturiation ratio
t	time, s
Ta	dimensionless Taylor number

$\langle u_i \rangle$	Reynolds averaged velocity in i^{th} direction, m/s
v	injection velocity, ml/min
V_i	injected volume, ml
V_r	reactor volume, ml
Y	reaction progress variable
Greek Letters	
Γ_t	turbulent diffusivity, m^2/s
γ_s	micromixing rate, 1/s
γ_t	spurious dissipation rate, 1/s
ϵ	turbulent dissipation rate, m^2/s^3
ν	kinematic viscosity, m^2/s
ξ	mixture fraction
ξ_s	stoichiometric mixture fraction
ρ	fluid density, kg/m^3
ρ_s	crystal density, kg/m^3
Ω_1	rotation speed of the inner cylinder, rad/s
Subscripts	
o	value in the inlet stream
Superscripts	
0	value in the case of mixing without reaction
∞	value in the case of infinitely fast reaction
$^{(n)}$	local value in mode n
Operators	
$\langle\rangle$	Reynolds average

References

Aoun. M., Plasari, E., David, R., and J. Villermaux, "Are Barium Sulphate Kinetics Sufficiently Known for Testing Precipitation Reactor Models?," *Chem. Eng. Sci.*, **51**, 2449 (1996).

Baldyga, J., and W. Orciuch, "Closure Problem for Precipitation," *Trans. Inst. Chem. Eng.*, **75A**, 160 (1997).

Baldyga, J., and W. Orciuch, "Closure Method for Precipitation in Inhomogeneous Turbulence," *Proceedings of the 14th Symposium on Industrial Crystallization*, 12-16 Sept, paper 86, Rugby, UK, 1069 (1999).

Baldyga, J., Pohorecki, R., Podgorska, W. and B. Marcant, "Micromixing Effects in Semibatch Precipitation," In A. Mersmann. (Ed.) *Proceeding of the 11th Symposium on Industrial Crystallization*, Garmisch-Partenkirchen, RFG, 175 (1990).

Baldyga, J., Podgorska, W., and R. Pohorecky, "Mixing Precitipitation Model with Application to Double Feed Semibatch Precipitation," *Chem. Eng. Sci.*, **50**, 1281 (1995).

Barresi, A.A., Marchisio, D., and G. Baldi, "On the Role of Micro- and Mesomixing in a Continuous Couette-Type Precipitator," *Chem. Eng. Sci.*, **54**, 2339 (1999).

Fitchett, D.E. and J.M. Tarbell, "Effect of Mixing on the Precipitation of Barium Sulphate in an MSMPR Reactor," *A.I.Ch.E. J.*, **36**, 511 (1990).

Fluent Inc. "Fluent 5 User's Guide," Fluent Inc., Lebanon, New Hampshire, USA (1990).

Fox, R.O., "The Spectral Relaxation Model of the Scalar Dissipation Rate in Homogeneous Turbulence," *Phys. Fluid*, **7**, 1082 (1995)

Fox, R.O., "Computational Methods for Turbulent Reacting Flows in the Chemical Process Industry," *Revue de l'Institute Francais du Petrole*, **51**, 215 (1996)

Fox, R.O., "The Langrangian Spectral Relaxation Model of the Scalar Dissipation Rate in Homogeneous Turbulence," *Phys. Fluid*, **9**, 2364 (1997)

Fox, R.O., "On the Relationship Between Lagrangian Micromixing Models and Computational Fluid Dynamics," *Chem. Eng. Proc.*, **37**, 521 (1998).

Fox, R.O., "The Lagrangian Spectral Relaxation Model for Differential Diffusion in Homogeneous Turbulence," *Phys. Fluid*, **11**, 1550 (1999)

Garside, J., and N.S. Tavare, "Mixing, Reaction and Precitipitation: Limits of Micromixing in an MSMPR Crystallizer," *Chem. Eng. Sci.*, **40**, 1485 (1985).

Kim, W.S., and J.M. Tarbell, "Micromixing Effects on Barium Sulphate Precipitation in a MSMPR Reactor," *Chem. Eng. Commun.*, **146**, 33 (1996).

Marchisio, D., Barresi, A.A., and G. Baldi, "Influence of the Hydrodynamics on the Solid Characteristics in a Couette Type Precipitator," *Proceedings of the 6th International Conference on Multiphase Flow in Industrial Plants*, Milan, Italy, 335 (1998).

Marchisio, D.L., Fox, R.O., Barresi, A.A., and G. Baldi, "A CFD Approach to Study the Local Importance of Aggregation in Precipitation," *Proceedings of the 7th International Conference on Multiphase Flow in Industrial Plants*, Bologna, Italy, in press (2000a)

Marchisio, D.L., Barresi, A.A., Baldi G., and R.O. Fox, "Comparison of Different Modelling Approaches to Turbulent Precipitation," *Proceeding 10th European Conference on Mixing*, (H.E.A. Van den Akker, Ed.), Delft, The Netherlands, July 2-5, in press (2000b).

Nielsen, A.E. "Nucleation and Growth of Crystal at High Supersaturation," *Kristall Technik*, **4**, 17 (1969).

Pagliolico, S., Marchisio, D., and A.A. Barresi, "Influence of Operating Conditions on $BaSO_4$ Crystal Size and Morphology in a Continuous Couette Precipitator," *J. Therm. Anal. Cal.*, **56**, 1423 (1999).

Phillips, R., Rohani, S., and J. Baldyga, "Micromixing in a Single-Feed Semi-Batch Precipitation Process," *A.I.Ch.E. J.*, **45**, 82 (1999).

Pipino, M., Barresi, A.A., and R.O. Fox "A PDF Approach to the Descripition of Homogeneous Nucleation," *Proceeding of the 4th International Conference on Multiphase Flow in Industrial Plants*, Ancona, Italy, 248 (1994).

Piton, D., Fox, R.O., and B. Marcant, "Simulation of Fine Particle Formation by Precipitation Using Computational Fluid Dynamics," *Canadian J. Chem. Eng.*, in press (2000).

Pohorecky, R., and J. Baldyga, "The Effect of Micromixing on the Course of Precipitation in an Unpremixed Feed Continuous Tank Crystallizer," *Proceeding of the 5th European Conference on Mixing* (BHRA), Wurzburg, West Germany, 105 (1985) .

Pohorecky, R., and J. Baldyga, "The Effect of Micromixing and the Manner of Reactor Feeding on Precipitation in Stirrer Tank Reactors," *Chem. Eng. Sci.*, **43**, 1949 (1988).

Randolph, A.D. and M.A. Larson, *Theory of Particulate Processes*, 2nd Ed., Academic Press, San Diego (1988).

Rivera, T., and A.D. Randolph, "A Model for the Precipitation of Pentaerythritol Tetranitrate (PETN)," *Ind. Eng. Chem. Process Des. Dev.*, **17**, 183 (1978).

Smith, G.P., and A.A. Townsend, "Turbulent Couette Flow Between Concentric Cylinders at Large Taylor Numbers," *J. Fluid Mech.*, **123**, 187 (1982).

Taylor, G.I. "Stability of a Viscous Liquid Contained Between Two Rotating Cylinders," *Phil. Trans. Roy. Soc. A*, **223**, 289 (1923).

Valerio S., Vanni M., Barresi A.A. and G. Baldi, "Engineering Modelling of Turbulent Flows in Chemical Engineering Applications," *Trends Chem. Eng.*, **5**, 1 (1998).

Wei, H., and J. Garside, "Application of CFD Modelling to Precipitation Systems," *Trans. Inst. Chem. Eng.*, **70A**, 219 (1997).